J. Fluid Mech. (1978), *vol.* 85, *part* 1, *pp.* 85–96
Printed in Great Britain

Propagation of perturbations in a gas–liquid mixture

By V. V. KUZNETSOV, V. E. NAKORYAKOV, B. G. POKUSAEV AND I. R. SHREIBER
Institute of Thermophysics, Siberian Branch of the USSR Academy of Sciences, Novosibirsk

(Received 22 September 1976 and in revised form 12 July 1977)

The present investigation has been performed over a wide range of the dimensionless parameters characterizing the process of propagation of pressure perturbations in a gas–liquid mixture; these are the Reynolds number, and a dispersion parameter responsible for the relation between the values of dispersion and signal intensity. The values of the above parameters were changed mainly by varying the initial perturbation. The results obtained show a complete agreement between the Burgers–Korteweg–de Vries model and the real process of propagation of long-wave perturbations in a liquid with gas bubbles. In addition to signal propagation with the formation of monotonic and oscillatory shock waves, the propagation of signals in the form of solitary waves (solitons) and wave packets was observed experimentally. Data have been obtained on signal damping, energy dissipation and the influence of mixture viscosity on the signal evolution.

1. Introduction

Great attention is being given to studying experimentally and theoretically the propagation of perturbations in a liquid with gas bubbles. Benjamin (1966), using general results of the nonlinear theory of wave propagation, was the first to predict the possibility of oscillatory shock-wave formation in a gas–liquid mixture (see also Batchelor 1969). He formulated some fundamental problems for further investigation. Wijngaarden (1968), using the Korteweg–de Vries equation, predicted the possibility of finite-duration signal propagation in the form of solitons and oscillatory wave packets. Nakoryakov, Sobolev & Shreiber (1972), Wijngaarden (1972), Noordzij (1973) and Nakoryakov *et al.* (1975 *b*) suggested that the propagation of perturbations in a liquid with gas bubbles should be considered on the basis of the Burgers–Korteweg–de Vries equation (BKV). The difference between the BKV and Korteweg–de Vries equations is that the former takes into account energy dissipation. Depending on the correlation between dissipation, wave dispersion, nonlinearity, signal duration and intensity, the BKV equation predicts the possibility of signal propagation in the form of shock waves, solitons, monotonic and oscillatory waves and formations shaped mainly by viscous forces.

Kutateladze *et al.* (1972) and Noordzij (1973) first showed the possibility of experimental realization of an oscillatory shock wave. Up to now the propagation of the signal in the form of solitons, wave packets and 'viscous' triangular profile formations in a liquid with gas bubbles has not been detected experimentally. The limits of applicability of Korteweg–de Vries, Burgers–Korteweg–de Vries and Burgers approxi-

mations have not been studied either. This article presents experimental results from a study aimed at the qualitative verification of the basic conclusions resulting from the theory of the above equations.

2. BKV approximation for perturbations in a liquid with gas bubbles

To describe the evolution of perturbations propagating in the same direction in a gas–liquid mixture the BKV equation was obtained by Nakoryakov *et al.* (1975*b*):

$$\partial u/\partial \tau + u[1+(\gamma+1)/2\phi_0](\partial u/\partial \xi) - \eta(\partial^2 u/\partial \xi^2) + \beta(\partial^3 u/\partial \xi^3) = 0, \tag{1}$$

where u is the velocity, τ the time, x the co-ordinate, $c_0 = (\gamma P_0/\rho_0\phi_0)^{\frac{1}{2}}$ is the low-frequency sound velocity, P is the pressure, ρ the density, ϕ the volumetric void fraction and γ the adiabatic exponent. The effective viscosity coefficient η, which is conditioned by viscous, acoustic and heat losses due to the pulsations of single inclusions, can be calculated using the work of Devin (1959), Nakoryakov *et al.* (1972) and Noordzij & Wijngaarden (1974). The formula is

$$\eta = 4\nu_l/3\phi_0(1-\phi_0) + \gamma R_0 c_0^2/c_l + [3(\gamma-1)/2](2a/\omega)^{\frac{1}{2}} c_0^2/\omega R_0, \tag{2}$$

where ν_l and c_l are, respectively, the kinematic viscosity of the liquid and the sound velocity in the liquid, ω is the resonant frequency of the bubbles, a the coefficient of thermal diffusivity in the gas, R_0 the radius of the equilibrium bubble and

$$\beta = R_0^2 c_0/6\phi_0(1-\phi_0)$$

the coefficient of dispersion. The subscript 0 here and elsewhere denotes the unperturbed state.

When considering nonlinear waves, we are able to proceed from the linearized hydrodynamic equations of Rudenko & Soluyan (1975). Thus the conditions of applicability of the BKV equation take the form

$$\Delta P/P_0 \sim u/c_0\phi_0 \sim \Delta\rho/\rho_0\phi_0 \sim \epsilon < 1. \tag{3}$$

Equation (1) is written in a co-ordinate system moving at speed c_0 and all the terms of the equation are of the same order of magnitude and of order ϵ^2. Hence one can pass from (1) to an equation for the pressure perturbation ΔP by a simple relation:

$$\Delta P = \int (\rho c)\, du \approx \rho_0 c_0 u + o(\epsilon^2). \tag{4}$$

For the pressure perturbations, (1) takes the form

$$\partial P/\partial \tau + [1+(\gamma+1)/2\phi_0](\Delta P/\rho_0 c_0)\,\partial P/\partial \xi - \eta\partial^2 P/\partial \xi^2 + \beta\,\partial^3 P/\partial \xi^3 = 0. \tag{5}$$

Introducing the function $P^* = [1+(\gamma+1)/2\phi_0]\Delta P/\rho_0 c_0$, we obtain an equation in the form

$$\partial P^*/\partial \tau + P^*\partial P^*/\partial \xi - \eta\partial^2 P^*/\partial \xi^2 + \beta\,\partial^3 P^*/\partial \xi^3 = 0. \tag{6}$$

This equation can readily be transformed to dimensionless form by introducing the length of the initial perturbation l_0 as a characteristic dimension and the amplitude of the initial perturbation $u_0(\xi)$ as a characteristic velocity uniquely related to the initial pressure perturbation in the mixture $\Delta P_0(\xi)$ by

$$u_0(\xi) = \Delta P_0(\xi)/\rho_0 c_0. \tag{7}$$

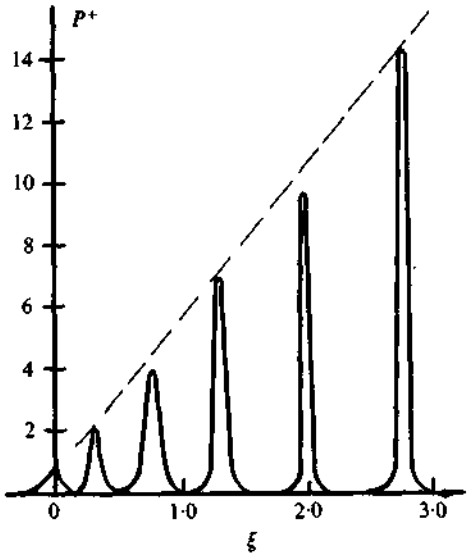

FIGURE 1. Perturbation profile for $\sigma > \sigma_c$ and $Re^{-1} = 0$.

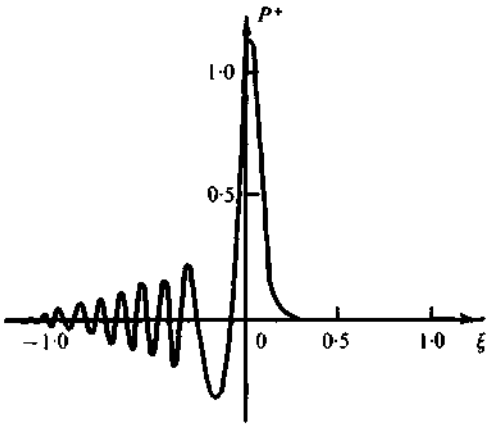

FIGURE 2. Perturbation profile for $\sigma < \sigma_c$ and $Re^{-1} = 0$.

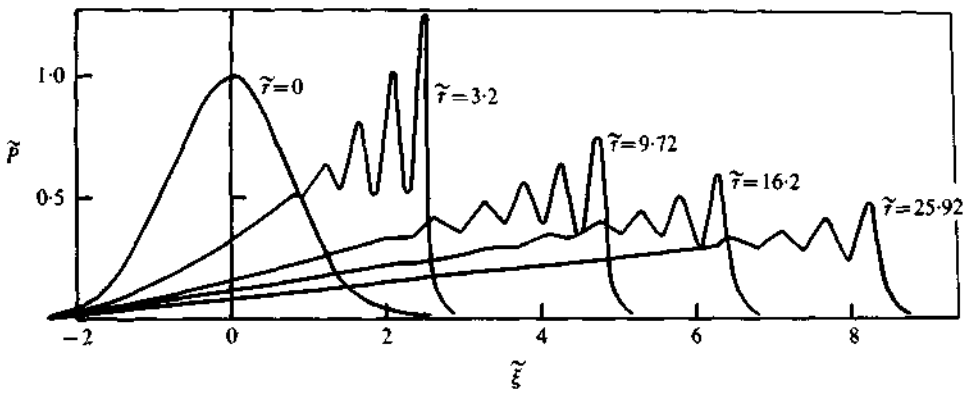

FIGURE 3. Perturbation profile for $\sigma = 30$ and $\sigma/Re = 0{\cdot}1$. Initial perturbation $\tilde{P}(0, \tilde{\xi}) = \exp(-\tilde{\xi}^2)$.

Equation (6) in its dimensionless form is

$$\partial\tilde{P}/\partial\tilde{\tau} + \tilde{P}\,\partial\tilde{P}/\partial\tilde{\xi} - Re^{-1}\partial^2\tilde{P}/\partial\tilde{\xi}^2 + \sigma^{-2}\partial^3\tilde{P}/\partial\tilde{\xi}^3 = 0. \tag{8}$$

Here

$$\tilde{\tau} = \tau u_0/l_0, \quad \tilde{\xi} = \xi/l_0, \quad Re = u_0 l_0/\eta, \quad \sigma = l_0(u_0/\beta)^{\frac{1}{2}},$$

$$\tilde{P} = P^*\rho_0 c_0/[1 + (\gamma+1)/2\phi_0]\Delta P_0 \equiv \Delta P/\Delta P_0.$$

At large Re or small σ, (8) takes the form of the Korteweg–de Vries equation:

$$\partial\tilde{P}/\partial\tilde{\tau} + \tilde{P}\,\partial\tilde{P}/\partial\tilde{\xi} + \sigma^{-2}\partial^3\tilde{P}/\partial\tilde{\xi}^3 = 0. \tag{9}$$

The basic properties of the solution of (9) which has been studied comprehensively are widely known (Berezin & Karpman 1966; Zabusky & Kruskal 1965). In particular, it is known that there exists a critical value of σ, which we denote by σ_c, at which

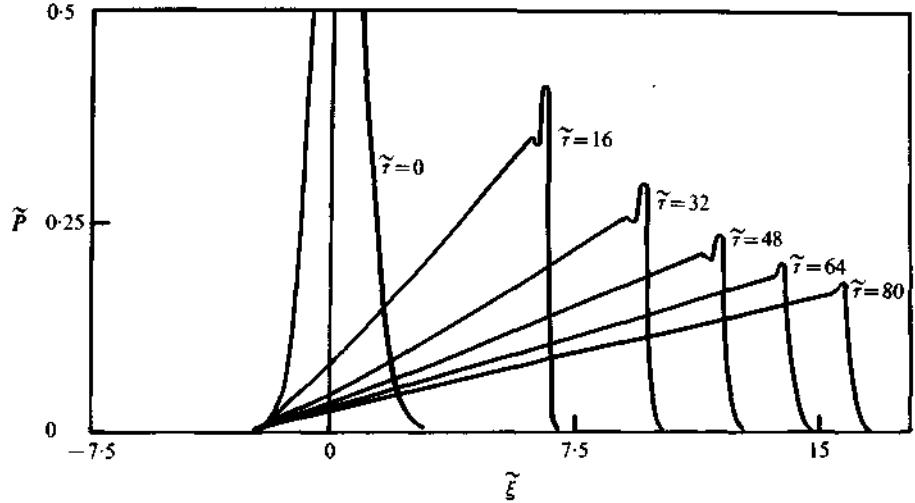

FIGURE 4. Perturbation profile for $\sigma = 50$ and $\sigma/Re = 0{\cdot}33$; $\tilde{P}(0, \tilde{\xi}) = \exp(-\tilde{\xi}^2)$.

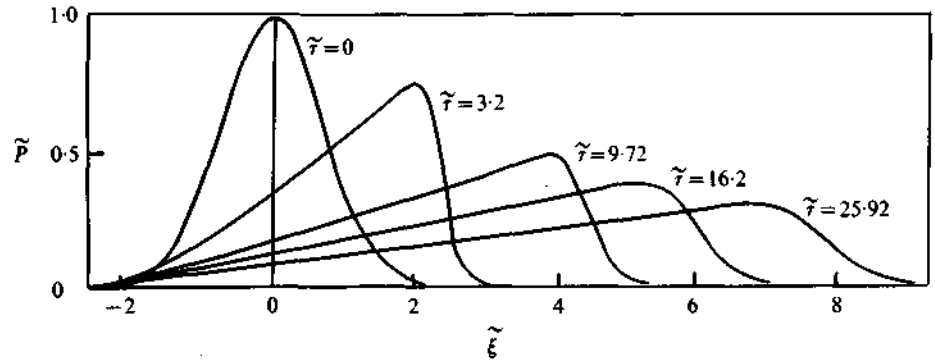

FIGURE 5. Perturbation profile for $\sigma = 30$ and $\sigma/Re = 1{\cdot}5$; $\tilde{P}(0, \tilde{\xi}) = \exp(-\tilde{\xi}^2)$.

the solutions of (9) change qualitatively (Berezin & Karpman 1966). Thus for $\sigma > \sigma_c$ the initial perturbation breaks up into solitons (figure 1), their number being determined by the value of the parameter σ. The value σ_c can be calculated for any kind of initial perturbation from Berezin & Karpman (1966). At $\sigma \ll \sigma_c$ the solutions have the form of an oscillatory wave packet (figure 2). At σ values close to σ_c, the initial perturbation breaks up into both solitons and wave packets. If the initial perturbation is negative, i.e. it is of the form of a dilatation wave, (9) has only wave packets as solution (Hammack & Segur 1974).

The above properties hold in the BKV equation as well. For this equation at $\sigma/Re \ll 1$ there is also a specific value $\sigma = \sigma_c$ which changes the structure of the solution.

With increasing σ/Re the nature of the solution of (8) changes qualitatively. Figure 3 shows the evolution of the initial perturbation with ξ at $\sigma/Re = 0{\cdot}1$. In this case the perturbation does not break up into single solitons but produces a wave with a triangular profile with an oscillating structure.

At large σ and small Re, (8) takes the form of the Burgers equation:

$$\partial\tilde{P}/\partial\tilde{\tau} + \tilde{P}\partial\tilde{P}/\partial\tilde{\xi} = (1/Re)\partial^2\tilde{P}/\partial\tilde{\xi}^2. \tag{10}$$

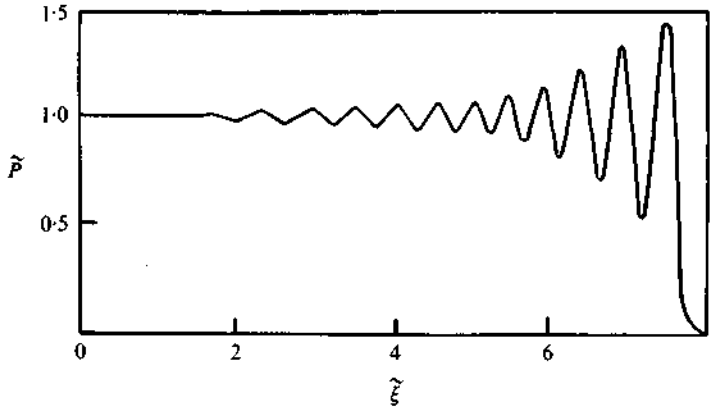

FIGURE 6. Perturbation profile for $\sigma = \infty$ and $\sigma/Re = 0{\cdot}1$. The initial perturbation is a 'step'.

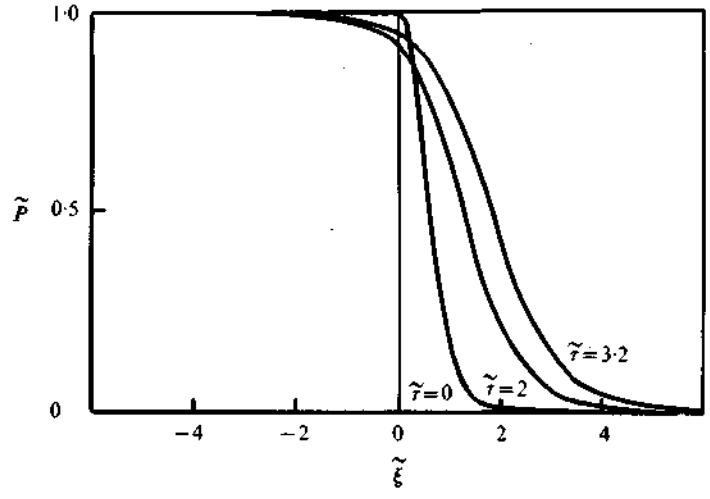

FIGURE 7. Perturbation profile for $\sigma = \infty$ and $\sigma/Re = 2$. The initial perturbation is a 'step'.

In accordance with (8), the signal, depending on the Reynolds number, either will propagate as a formation which is blurred by the linear equation of thermal diffusivity or will become steeper resulting in a shock discontinuity (Rudenko & Soluyan 1975).

Figures 4 and 5 represent the results of integrating (8) first for $\sigma/Re = 0{\cdot}33$ and $\sigma = 50$, and second for $\sigma/Re = 1{\cdot}5$ and $\sigma = 30$. As is seen, even though $\sigma > \sigma_c$, no break-up of the perturbation into solitons is observed and the perturbation evolves (figure 4) according to the nature of the solution of (10).

Equations (9) and (10) do not provide solutions of the oscillatory shock-wave type. This solution can be obtained from (8) only.

The analysis by Sagdeev (1964) of a stationary form of (1) in which the perturbation evolved only in time (for application to plasma waves) showed the possibility of the formation of stationary shock waves of monotonic and oscillatory structure. The criterion that determines which structure is realized is: for $\sigma/Re > \sqrt{2}$, the structure is monotonic and for $\sigma/Re < \sqrt{2}$ it is oscillatory.

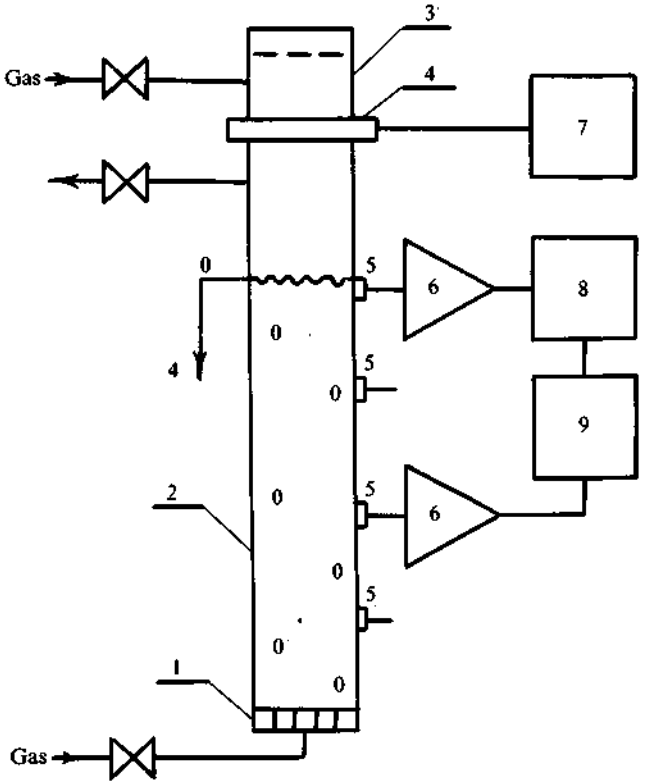

FIGURE 8

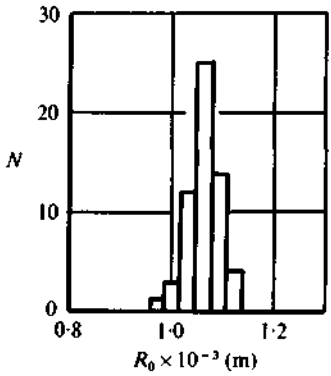

FIGURE 9

FIGURE 8. Schematic diagram. (1) Bubble generator. (2) Test section. (3) High-pressure chamber. (4) Diaphragm fixing. (5) Pressure transducer. (6) Intensifier. (7) Diaphragm breaker. (8) Pulse delay line. (9) Oscilloscope.

FIGURE 9. Distribution of bubble sizes. CO_2, $R_0 = (1{\cdot}06 \pm 0{\cdot}03) \times 10^{-3}$ m.

Nakoryakov *et al.* (1975*b*) using numerical integration of (8) showed the above criterion to be applicable to the analysis of non-stationary shock waves in a liquid with gas bubbles. An example of the numerical integration of (8) at $\sigma/Re = 0{\cdot}1$ and $\sigma/Re = 2$ is presented in figures 6 and 7, respectively. Nigmatulin, Khabeev & Shagapov (1974) also investigated numerically the shock-wave structure in a gas–liquid medium.

3. Experimental study of the structure and dynamics of perturbations

To clarify the nature of perturbation propagation in a gas–liquid mixture for σ greater than and less than its critical value σ_c, laboratory experiments were carried out with the set-up schematically shown in figure 8. The vertical tube is 53 mm I.D. and 3 m long. Along the working section (2), which is optically transparent, piezoelectric pressure transducers are placed flush with the tube wall. The transducer signal was displayed on the oscillograph and then processed. The velocity of the perturbation propagation was determined by the time taken for the pressure perturbation to traverse the distance between two probes. The medium under study which

Figure	L (m)	$P_0 \times 10^5$ (N/m^2)	$R_0 \times 10^3$ (m)	$\phi_0 \times 10^2$	ΔP_0 (bar)	l_0 (m)	σ	Re	σ/Re	$\Delta P_m/\Delta P_0$	Signal characteristics
(*a*)	0	1	1·41	1·11	0·48	0·1	12·1	—	—	—	Characteristic shape of initial pulse
(*b*)	0·6	1·07	1·38	1·03	0·35	0·9	—	—	0·05	1·28	Shock wave
(*c*)	1·4	1·16	1·34	0·95	0·945	0·2	52·8	3520	0·015	0·34	Multi-soliton perturbation
(*d*)	1·4	1·16	1·34	0·95	0·48	0·16	30	1500	0·021	0·37	Two-soliton perturbation
(*e*)	0·6	1·07	1·38	1·03	0·29	0·1	12·1	356	0·034	0·61	Single soliton
(*f*)	0·6	1·07	1·38	1·03	0·035	0·06	3·4	48	0·071	0·28	Wave packet

TABLE 1. Parameters for figure 10.

filled the test section of the tube was generated by saturating the working liquid with gas bubbles by means of a bubble generator (1) located in the lower part of the tube. A water–glycerine solution with $\nu_l = 1{\cdot}8 \times 10^{-5}\,\mathrm{m^2/s}$ and $\rho_l = 1{\cdot}18 \times 10^3\,\mathrm{kg/m^3}$ used as a working liquid made it possible to produce spherical bubbles of practically the same size slowly emerging at a velocity of 2–3 cm/s. The histogram of the distribution of bubble sizes is presented in figure 9. Bubble size was measured photographically and cinematographically. The average volumetric void fraction was determined by the change in the height of the liquid column when introducing gas bubbles. The local values of ϕ_0 and R_0 in the test section were calculated from the observed average value of ϕ and from a measured R, assuming a hydrostatic pressure distribution in the mixture under isothermal conditions, taking account of the hydrostatic liquid column.

Carbon dioxide and helium, with coefficients of thermal diffusivity a equal to $1{\cdot}03 \times 10^{-5}\,\mathrm{m^2/s}$ and $18{\cdot}1 \times 10^{-5}\,\mathrm{m^2/s}$, respectively, were used as working gases. The use of different gases ensures more than a ten-fold change in the coefficient of the effective viscosity η (when we remember that γ changes as well as a).

The perturbing pulse was produced by breaking the diaphragm (3) separating the high-pressure chamber (4) from the test section. By changing the length of the high-pressure chamber, it is possible to vary the duration of the initial pulse l_0 and to study the features of the propagation of both the shock waves and the finite pressure perturbation in a gas–liquid medium. The diaphragm was placed at a distance of 1 m from the upper level of the medium, so that the reflected waves did not influence the structure of the signal investigated.

Figure 10 (plate 1) shows characteristic oscillograms of the pressure perturbation in a liquid with CO_2 bubbles, while table 1 lists the parameters of the perturbations; here ΔP_0 is the intensity of the initial pressure perturbation, ΔP_m is the current intensity and L is the distance from where the perturbation entered the medium. Figure 10(a) represents the characteristic shape of the initial perturbation which can further develop into the perturbations shown in the oscillograms of figures 10(c–f). The oscillogram of figure 10(b) pertains to the step perturbation. The critical value σ_c for the initial perturbation in figure 10(a) is equal to 14. As seen from table 1, the condition $\sigma/Re \ll 1$ was met for all the experiments presented in figures 10(c–f) and in this case the evolution of the pressure perturbations is in good agreement with the main conclusions of the theory for equation (9).

Indeed, at $\sigma > \sigma_c$ the initial perturbation breaks up into a sequence of solitons (figures 10c, d) whose number can be found from the formula (Berezin & Karpman 1966)

$$N = 2\sigma/3\pi\sqrt{6}. \tag{11}$$

Thus at $\sigma = 53$, from (11) it follows that $N = 5$; this corresponds to the number of solitons observed experimentally, see figure 10(c). With a decrease in σ the number of solitons diminishes, as in figure 10(d), and at $\sigma \approx \sigma_c$ the initial perturbation produces only one soliton, as in figure 10(e). At $\sigma \ll \sigma_c$ the initial perturbation transforms into an oscillatory wave packet (figure 10f).

Figure 11 shows experimental results on the way the velocity of solitons and wave packets in a liquid with CO_2 bubbles depends on their amplitude. The perturbation velocity averaged over a 0·8 m segment was measured. The middle of this segment was as far as 1 m from the upper level of the medium. Presented here also is a calculation

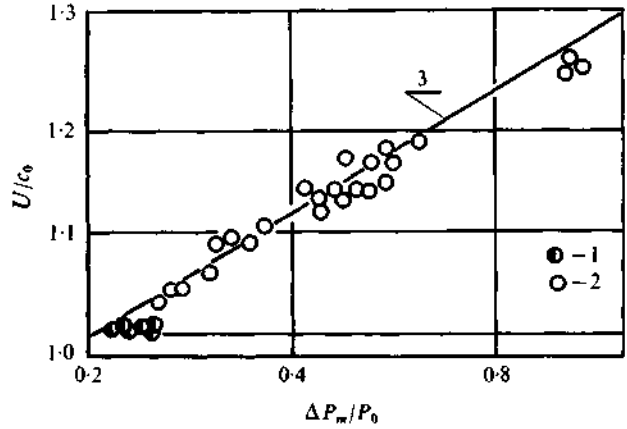

FIGURE 11. Velocity of pressure perturbation in a liquid with CO_2 bubbles. $R_0 = 1{\cdot}36 \times 10^{-3}$ m; $\phi_0 = 0{\cdot}99 \times 10^{-2}$; $P_0 = 1{\cdot}11 \times 10^5$ N/m^2; $c_0 = 109$ m/s. (1) Wave packet. (2) Soliton. (3) Calculation from (12) at $\gamma = 1{\cdot}22$.

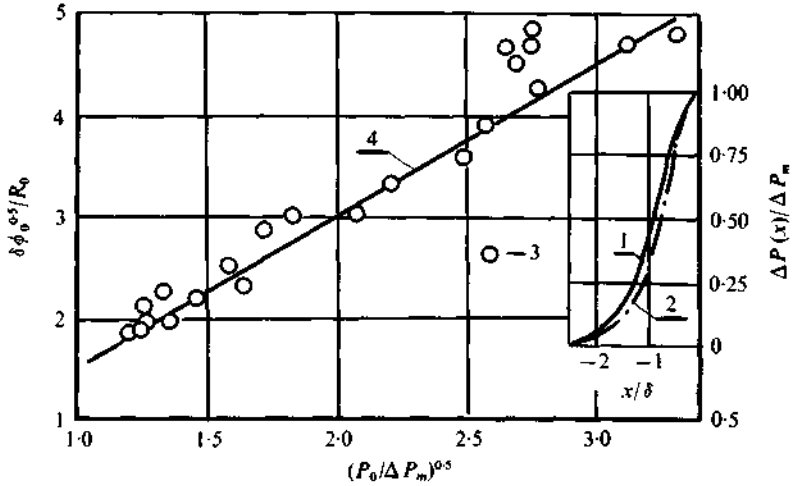

FIGURE 12. Dependence of the half-width of solitons on their amplitude. (1), (3) Experiment at $L = 0{\cdot}6$ m, $P_0 = 1{\cdot}07 \times 10^5$ N/m^2, $R_0 = 1{\cdot}38 \times 10^{-3}$ m, $\phi_0 = 1{\cdot}03 \times 10^{-2}$. (2) Calculation from (13) for $\gamma = 1{\cdot}3$. (4) Calculation from (14) for $\gamma = 1{\cdot}3$.

from the known dependence (Berezin & Karpman 1966) for the velocity of solitons, which for a gas–liquid medium is of the form

$$U = c_0[1 + (\gamma + 1)\Delta P_m/6\gamma P_0], \tag{12}$$

where ΔP_m is the amplitude of the solitary wave. Formula (12) describes the experimental results at $\gamma = 1{\cdot}22$. This is close to the value of the adiabatic exponent for CO_2, $\gamma = 1{\cdot}3$. From the diagram it also follows that the velocity of wave packets is close to the low-frequency speed of sound in the medium.

Figure 12 presents, in dimensionless co-ordinates, the dependence of the half-width of a solitary wave upon the perturbation intensity and it also presents a comparison of the experimental wave profile with the theoretical shape of the soliton

$$\Delta P(x) = \Delta P_m \sec h^2(x/\delta), \tag{13}$$

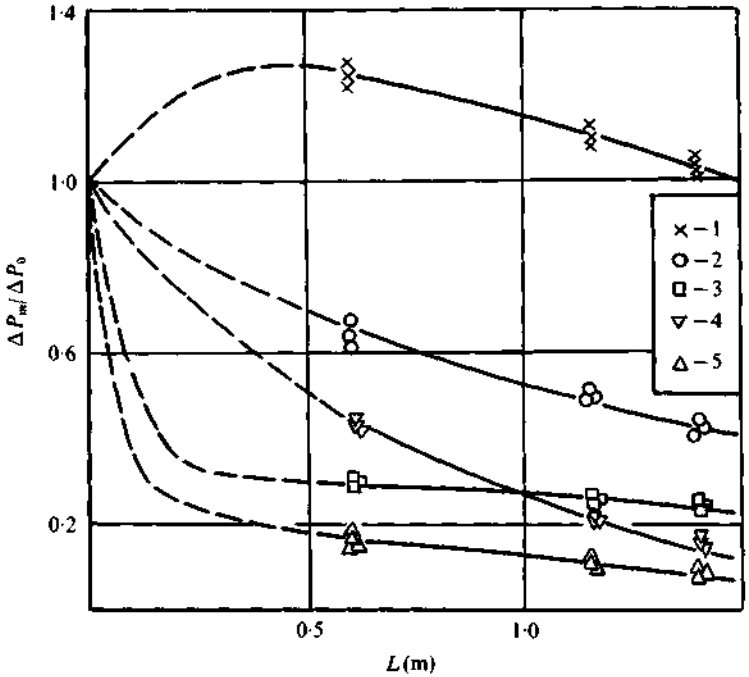

FIGURE 16. Variation of the perturbation amplitude along the working section. Gas CO_2; $L = 0$; $P_0 = 10^5$ N/m²; $R_0 = 1{\cdot}41 \times 10^{-3}$ m; $\phi_0 = 1{\cdot}11 \times 10^{-2}$. (1) Shock wave, $\Delta P_0 \approx 0{\cdot}3 \times 10^{-5}$ N/m². (2) Single soliton, $\Delta P_0 \approx 0{\cdot}4 \times 10^5$ N/m², $\sigma \approx 11$. (3) Wave packet, $\Delta P \approx 0{\cdot}13 \times 10^5$ N/m², $\sigma \approx 3{\cdot}1$, gas He, $L = 0$, $P_0 = 10^5$ N/m², $R_0 = 1{\cdot}27 \times 10^{-3}$ m, $\phi_0 = 1{\cdot}11 \times 10^{-2}$. (4) Soliton, $\Delta P_0 = (0{\cdot}3 \div 0{\cdot}5) \times 10^5$ N/m², $\sigma \approx 11$. (5) Wave packet, $\Delta P_0 = (0{\cdot}09 \div 0{\cdot}16) \times 10^5$ N/m², $\sigma \approx 2{\cdot}2$.

where the half-width of the soliton, determined at the level $0{\cdot}42\,\Delta P_m$, is equal to

$$\delta = [4\gamma/(\gamma+1)]^{\frac{1}{4}}(P_0/\Delta P_m)^{\frac{1}{4}} R_0/\phi_0^{\frac{1}{2}}. \tag{14}$$

The character of the evolution of an initially triangular perturbation in a liquid with He bubbles is shown in figures 13–15 (plates 2 and 3). The use of He bubbles enables one to obtain high values of σ/Re owing to the appreciably increased η. As seen from the oscillograms presented, the dissipative losses greatly influence the amplitude and the structure of pressure perturbations. Thus for $\sigma > \sigma_c$ (figure 13) the initial perturbation does not break up into solitary waves as in the case $\sigma/Re \ll 1$, but produces an oscillatory shock wave of triangular profile with length-damped oscillations.

For $\sigma \approx \sigma_c$ (figure 14) a soliton produced in this medium tends to spread out, the front edge naturally spreading out much slower. The formation of the wave packet at small $\sigma \ll \sigma_c$ (figure 15) is barely discernible, and the initial pulse is likely to spread out according to the solution of the Burgers linear equation.

Figure 16 presents the variations in the signal intensity along the tube in media with He and CO_2 bubbles. Given here are the experimental results for wave packets ($\sigma \ll \sigma_c$), single solitons ($\sigma \lesssim \sigma_c$) and shock waves formed by an initial step perturbation. A very strong decrease in the signal intensity takes place during the formation of wave packets. In this case the formation zone, shown qualitatively as dashed lines in the plot, produces an 'atomization' of the initial perturbation with the conservation

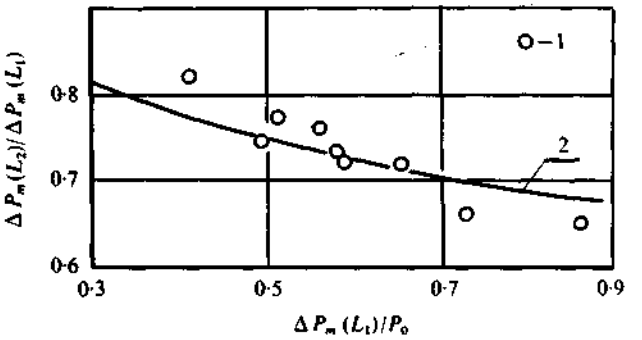

FIGURE 17. Damping of the soliton amplitude with length. Gas CO_2, $L_1 = 0{\cdot}6$ m, $L_2 = 1{\cdot}4$ m. (1) Experiment. (2) Calculation from (15) for $\alpha = 6\,s^{-1}$, $\eta = 3{\cdot}3\times10^{-2}$ m²/s, $\gamma = 1{\cdot}3$, $\beta = 0{\cdot}34\times10^{-2}$ m²/s.

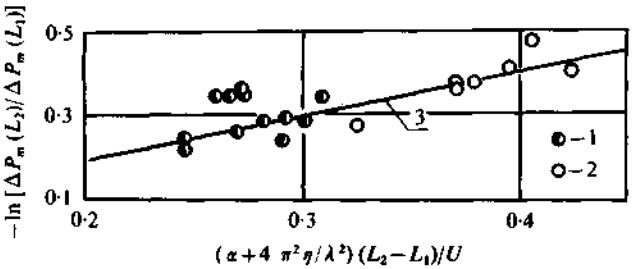

FIGURE 18. Damping of the wave packet along the test section. Gas CO_2; $\sigma \ll \sigma_c$. Experiment: (1) $L_1 = 0{\cdot}6$ m, $L_2 = 1{\cdot}4$ m; (2) $L_1 = 0{\cdot}63$ m, $L_2 = 1{\cdot}78$ m. (3) Calculation from (16) for $\eta = 2{\cdot}9\times10^{-2}$ m²/s, $\alpha = 6\,s^{-1}$, $\gamma = 1{\cdot}3$.

of its pulse. With a shock wave the reconstruction of the perturbation structure produces an oscillatory shock wave, the amplitude of the first oscillation being greater than the pressure gradient in the initial perturbation (figure 16, graph (1)). The damping of the solitons and wave packets is conditioned by dissipative losses. In fact, in a liquid with He bubbles (figure 16, graphs (4) and (5)) the pressure perturbations damp more intensively than they would if the bubbles contained CO_2 (figure 16, graphs (2) and (3)).

Figures 17 and 18 show experimental results on the damping of solitons and wave packets formed in a liquid with CO_2 bubbles. Measurements were carried out in a 0·8 m segment. As is seen, the damping of solitons is adequately described by a relation due to Pelinovsky (1971) and Otto & Sudana (1970) with $\eta = 3{\cdot}3\times10^{-2}$ m²/s:

$$\Delta P_m(L_2) = \Delta P_m(L_1)\exp(-4\alpha\Delta L/3U) \times\{1+(\gamma+1)c_0\Delta P_m(L_1)\eta[1-\exp(-4\alpha\Delta L/3U)]/30\gamma\alpha\beta P_0(L_1)\}^{-1}. \quad (15)$$

The damping of wave packets is described by a formula due to Pelinovsky (1971) with $\eta = 2{\cdot}9\times10^{-2}$ m²/s:

$$\Delta P_m(L_2) = \Delta P_m(L_1)\exp[-(\alpha+4\pi^2\eta/\lambda^2)\Delta L/U]. \quad (16)$$

Here $\alpha = \rho g c_0 / 2P_0(L_1)$ is the low-frequency absorption factor taking account of the density variation with the tube height, which can be calculated as is done by Noordzij & Wijngaarden (1974); λ is the wave-packet wavelength.

The analysis of the plots in figures 17 and 18 shows that from a rough account of the dissipative losses via the damping decrement of the inherent bubble oscillation the effective viscosity coefficient for the medium can be evaluated. Also it is the first time that pulse propagation in a medium containing bubbles has been detected as solitary waves and wave packets. The long-wave perturbation in this medium is shown to obey the regularities resulting from the theory of the Korteweg–de Vries–Burgers equation. The results obtained may be used to analyse the dynamics of waves passing through two-phase media and to simulate plasma processes by those in gas–liquid media.

The authors acknowledge the assistance of Gasenko V.G. (Institute of Thermophysics, Siberian Branch of the USSR Academy of Science), who kindly supplied the results of the numerical calculation of the BKV equation.

REFERENCES

Batchelor, G. K. 1969 In *Fluid Dynamics Transaction*, vol. IV (ed. W. Fiszdon, P. Kucharczyk & W. I. Prosnak), p. 425. Warszaw: PWN.

Benjamin, T. B. 1966 *Proc. 6th Symp. Naval Hydrodyn.* (ed. R. D. Cooper & S. W. Doroff), p. 121. Washington: Office Naval Res.

Berezin, Yu. A. & Karpman, V. I. 1966 *Zh. Eksp. i Teor. Fiz.* **51**, 1557.

Devin, C. 1959 *J. Acoust. Soc. Am.* **31**, 1654.

Hammack, J. L. & Segur, H. 1974 *J. Fluid Mech.* **65**, 289.

Kutateladze, S. S. *et al.* 1972 *Dokl. Akad. Nauk USSR* **207**, 313.

Nakoryakov, V. E. *et al.* 1975 In *Wave Processes in Two-Phase Media* (ed. S. S. Kutateladze), p. 54. Novosibirsk: Inst. Thermophys., Siberian Branch USSR Acad. Sci.

Nakoryakov, V. E., Sobolev, V. V. & Shreiber, I. R. 1972 *Izv. Akad. Nauk USSR, Mekh. Zh. i Gaza* **5**, 71.

Nakoryakov, V. E., Sobolev, V. V. & Shreiber, I. R. 1975 In *Wave Processes in Two-Phase Media* (ed. S. S. Kutateladze), p. 5. Novosibirsk: Inst. Thermophys., Siberian Branch USSR Acad. Sci.

Nigmatulin, R. I., Khabeev, N. S. & Shagapov, V. Sh. 1974 *Dokl. Akad. Nauk USSR* **214**, 779.

Noordzij, L. 1973 *Proc. IUTAM Symp. Non-Steady Flow of Water at High Speeds* (ed. L. I. Sedov & G. Yu. Stepanov), p. 369. Moscow: Nauka.

Noordzij, L. & Wijngaarden, L. van 1974 *J. Fluid Mech.* **66**, 115.

Otto, E. & Sudana, R. N. 1970 *Phys. Fluids* **13**, 1432.

Pelinovsky, E. N. 1971 *Zh. Prikl. Mekh. i Tech. Fiz.* **2**, 80.

Rudenko, O. V. & Soluyan, S. I. 1975 *Theoretical Fundamentals of Non-Linear Acoustics.* Moscow: Nauka.

Sagdeev, R. Z. 1964 *Some Points of Plasma Theory*, no. 4, p. 20. Moscow: Atomizdat.

Wijngaarden, L. van 1968 *J. Fluid Mech.* **33**, 465.

Wijngaarden, L. van 1972 *Ann. Rev. Fluid Mech.* **4**, 369.

Zabusky, N. J. & Kruskal, M. D. 1965 *Phys. Rev. Lett.* **15**, 240.

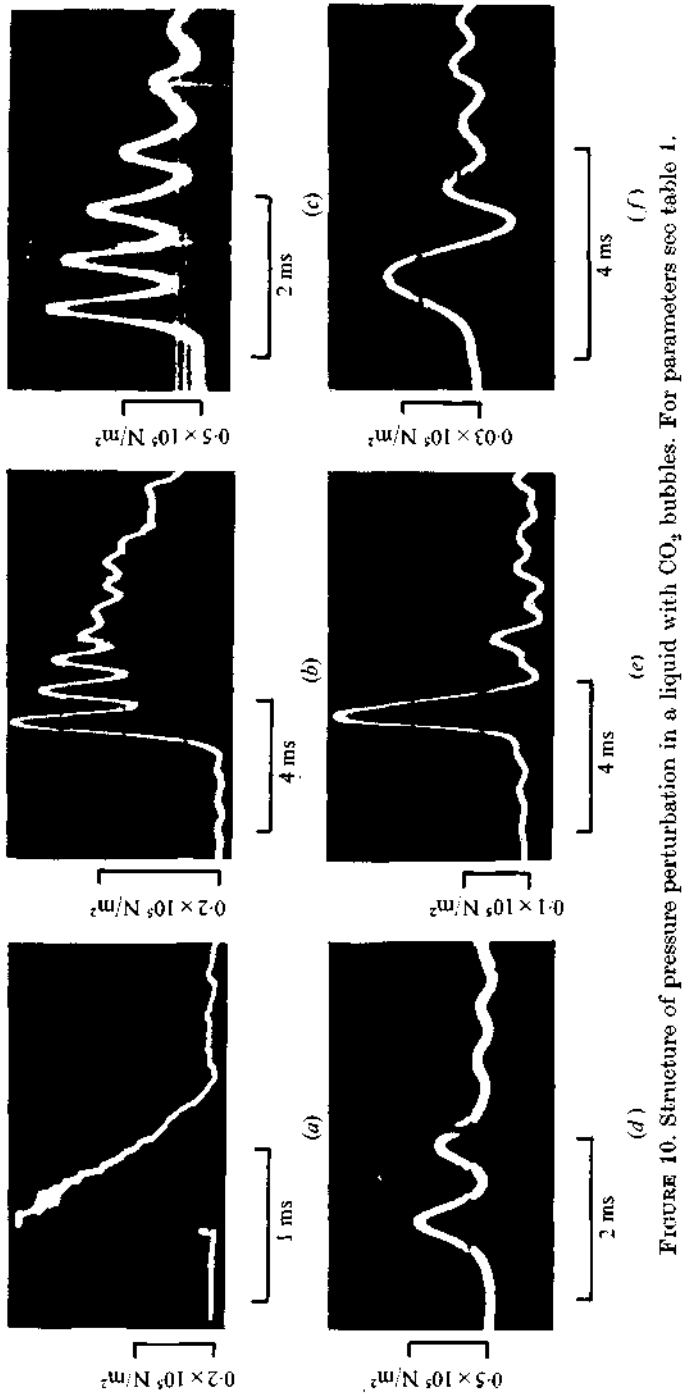

FIGURE 10. Structure of pressure perturbation in a liquid with CO_2 bubbles. For parameters see table 1.

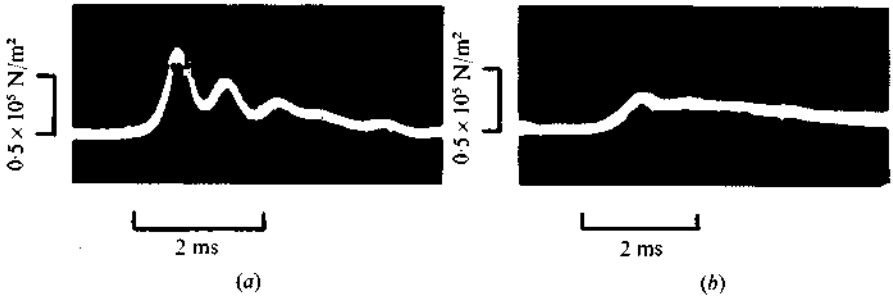

FIGURE 13. Evolution of the multi-soliton perturbation in a liquid with He bubbles. $\sigma = 36$; $\sigma/Re = 0{\cdot}14$; $\Delta P_0 = 1{\cdot}74 \times 10^5$ N/m²; $l_0 = 0{\cdot}15$ m.

	L (m)	$P_0 \times 10^{-5}$ (N/m²)	$\phi_0 \times 10^2$	$R_0 \times 10^3$ (m)	$\Delta P_0/\Delta P_0$
(*a*)	0·6	1·07	1·03	1·24	0·47
(*b*)	1·4	1·16	0·95	1·21	0·16

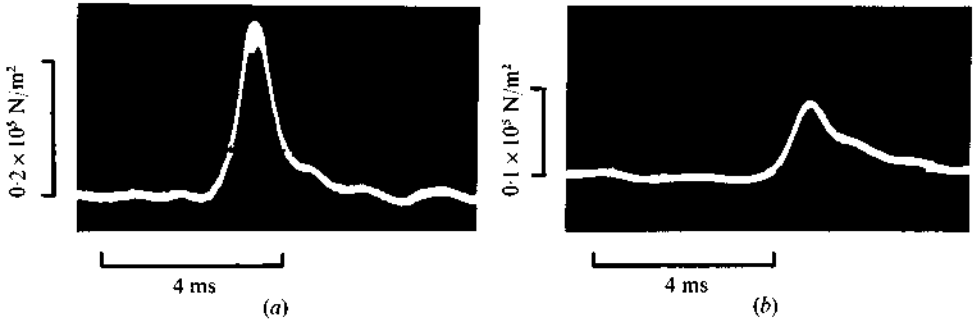

FIGURE 14. Evolution of a single soliton in a liquid with He bubbles. $\sigma = 13{\cdot}1$; $\sigma/Re = 0{\cdot}21$; $\Delta P_0 = 0{\cdot}628 \times 10^5$ N/m²; $l_0 = 0{\cdot}09$ m.

	L (m)	$P_0 \times 10^{-5}$ (N/m²)	$R_0 \times 10^3$ (m)	$\phi_0 \times 10^2$	$\Delta P_m/\Delta P_0$
(*a*)	0·6	1·07	1·24	1·03	0·415
(*b*)	1·4	1·16	1·21	0·95	0·149

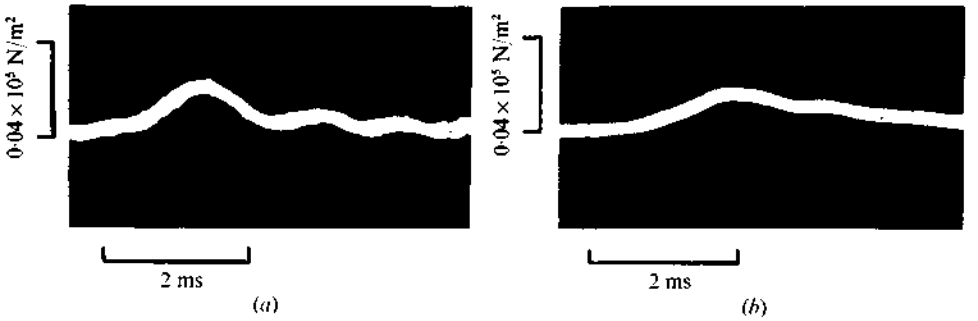

FIGURE 15. Evolution of perturbation at $\sigma < \sigma_c$ in a liquid with He bubbles. $\sigma = 2{\cdot}2$; $\sigma/Re = 0{\cdot}46$; $\Delta P_0 = 0{\cdot}148 \times 10^5$ N/m²; $l_0 = 0{\cdot}033$ m.

	L (m)	$P_0 \times 10^{-5}$ (N/m²)	$R_0 \times 10^3$ (m)	$\phi_0 \times 10^2$
(*a*)	0·6	1·07	1·24	1·03
(*b*)	1·15	1·13	1·22	0·98